

Simulations of the periodic flaring rate on YY Gem

D. H. Gao^{*}, P. F. Chen[†], M. D. Ding[‡], X. D. Li

Department of Astronomy, Nanjing University, Nanjing 210093, China

Accepted –. Received –; in original form –

ABSTRACT

The binary YY Gem shows many interesting properties, one of which is the periodicity in its flaring rate. The period, which is about 48 ± 3 min, was ever interpreted in terms of the oscillation of a filament. In this paper, we propose a new model to explain this phenomenon by means of 2.5-dimensional MHD numerical simulations. It is found that magnetic reconnection is induced as the coronal loops rooted on both stars inflate and approach each other, which is driven by the differential stellar rotation. The magnetic reconnection is modulated by fast-mode magnetoacoustic waves which are trapped between the surfaces of the two stars, so that the reconnection rate presents a periodic behaviour. With the typical parameters for the binary system, the observed period can be reproduced. We also derive an empirical formula to relate the period of the flaring rate to the coronal temperature and density, as well as the magnetic field.

Key words: binaries: close – stars: flare – stars: oscillations – waves – methods: numerical

1 INTRODUCTION

The binary system YY Gem has been studied for many years since discovered (Adams & Joy 1920). It is a double-lined spectroscopic eclipsing binary system which contains two dM1e late-type stars with masses and radii almost identical, and the orbital period being 0.8142822 d (Joy & Sanford 1926; van Gent 1931). It is of great importance to study the basic relations of such rare late-type binaries (Kron 1952; Butler, Doyle & Budding 1996). Based on some considerations in Dworak (1975), Brancewicz & Dworak (1980) gave the parameters of YY Gem: $M_1 = M_2 = 0.57 M_\odot$, $R_1 = R_2 = 0.6 R_\odot$, the separation of the two components $a = 3.83 R_\odot$.

Chabrier & Baraffe (1995) demonstrated that the depth of each stellar radiative core is ~ 70 per cent of its radius, and the thickness of the convective zone is ~ 30 per cent. Strong convective motions under the surfaces cause large-scale star spots and huge magnetic field structures. Flare activity on YY Gem was reported for the first time by Moffett & Bopp (1971). Subsequent investigations have shown that it is one of the most active flaring binaries (Moffett 1974; Doyle & Butler 1985; Doyle et al. 1990). Their flaring activities have been studied in multi-wavelengths. Using the Very Large Array, Jackson, Kundu & White (1989) presented radio observations; Stelzer et al. (2002) studied the simultaneous X-ray

spectroscopy of YY Gem with *Chandra* and *XMM-Newton* satellites; While, far UV observations of YY Gem were reported by Saar & Bookbinder (2003). The flarings on YY Gem exhibit UV and X-ray emissions which are stronger than those on the Sun (Haisch et al. 1990). For example, Tsikoudi & Kellett (2000) observed two large flares, and the integrated X-ray luminosity was estimated to be about $6\text{--}8 \times 10^{33}$ erg. They also calculated the ratio of X-ray and bolometric luminosities L_X/L_{Bol} , which indicated strong magnetic activities and ‘hot’ coronal components.

For close binaries with similar masses, the density scale-height is quite large, i.e., the density does not decrease with height from the stellar surfaces as rapidly as in the solar corona. Therefore, the hot plasma between the two stars could emit strong X-ray light. For example, observations revealed large-scale strong X-ray sources between the two stars of the RS CVn binary AR Lac (Siarkowski 1992; Siarkowski et al. 1996), as well as of the RS CVn binary TY Pyx (Culhane et al. 1990; Pres, Siarkowski & Sylwester 1995). At the same time, it is probable that the two stars are magnetically connected, as illustrated by Uchida & Sakurai (1983). Uchida & Sakurai (1985) proposed that the interstellar activities are intimately affected by the differential rotations of both stars. So, there may exist some interesting phenomena in such a system. One of them is the periodic flaring rate, which was reported by Doyle et al. (1990). Their observation in the *U*-band showed four flares separated in succession with a periodicity of 48 ± 3 min during a total observing time of 408 min. The duration of each flare varies from ~ 20 min to ~ 40 min, and the time-averaged flare luminosity in the *U*-band is 1.25×10^{28} erg s^{-1} . They in-

* E-mail: mg0526001@smail.nju.edu.cn

† chenpf@nju.edu.cn

‡ dmd@nju.edu.cn

terpreted this periodicity in terms of filament oscillations. In this paper, we attempt to propose an alternative explanation for the periodicity.

Flares on the Sun and dKe-dMe stars are both thought to result from magnetic reconnection. On the Sun, periodic behaviours have also been reported in various reconnection-associated phenomena, e.g., the quasi-periodic modulation of flaring emission (Nakariakov et al. 2006) and the repetitive appearance of transition region explosive events (Chen & Priest 2006). In the former case, magnetic reconnection is modulated by magnetoacoustic waves from a nearby oscillating coronal loop, whereas in the latter, magnetic reconnection is modulated by p -mode waves.

To our knowledge, no efforts in MHD numerical simulations have been devoted to the investigation of flaring phenomenon in binary systems, although hydrodynamic simulations have been done regarding flares in M dwarf stars (e.g. Cheng & Pallavicini 1991). Using potential field extrapolation, Uchida & Sakurai (1985) demonstrated that the evolving surface magnetic field can result in magnetic reconnection in the interstellar space. Here, we perform MHD numerical simulations in order to investigate the magnetic reconnection in a close binary system, with the purpose to clarify which process is likely to be responsible for the periodicity of the flaring rate as reported by Doyle et al. (1990). The paper is organised as follows. Section 2 describes the basic model, MHD equations, initial and boundary conditions. Section 3 gives the numerically calculated results. Discussions are presented in section 4, which is followed by conclusions in section 5.

2 NUMERICAL METHOD

2.1 Problem setup

The basic model used in our work is shown in Fig. 1. For ordinary binaries, the member stars are usually of different types. As usual, we call the one with larger mass the primary, marked as M_1 , the other the secondary, marked as M_2 ($M_1 > M_2$). Owing to the difference in mass, the point of zero gravity and the centre of mass are located at different positions. The former is closer to the secondary (M_2) and the latter is closer to the primary (M_1). In the case of YY Gem, we take the parameters given by Brancewicz & Dworak (1980), i.e., $M_1 = M_2$, so that the two points are actually cospatial. As shown in Fig. 1, a is the separation of two stellar centres, and $D = 2.63 R_\odot$ is the distance between the two surfaces along the joint line of the stars.

Because of the short orbital period, Struve & Zeberg (1959) and Qian et al. (2002) suggested that YY Gem should be in synchronized rotation. Therefore, we assume that the angular velocities of both stars have the same value as that of the co-rotating reference system. This means that the two stars rotate almost face to face except the differential rotation. As a result of the differential rotation, persistent shear motion is imposed to the coronal loops whose footpoints are rooted at different latitudes.

The MHD processes driven by the differential rotation are three-dimensional in nature. The addition of the two spherical boundaries makes the problem more unfeasible to solve numerically. To simplify the problem without losing

the essence of physics, the spherical boundaries are treated as two parallel planes, which are tangent to the spheres at the equators as illustrated with the dotted lines in Fig. 1. The area of interest is $0 \leq x \leq D$ and $-2.5 R_\odot \leq y \leq 2.5 R_\odot$, where the x -axis is along the joint line of the binary, the y -axis is parallel to the axis of the rotation, and the z -axis is perpendicular to the $x - y$ plane, with the origin of the coordinate being located on the equator of M_1 star. Note that the vertical size is set to be larger than the stellar radius in order to minimize the influence of the top boundary on the numerical results. Moreover, all quantities are approximated to be invariant along the z -axis, so that the problem becomes 2.5-dimensional. In reality, the interface between the magnetic systems of the two stars has a limited extension in the z -direction. Therefore, it should be kept in mind that any feature in our numerical results should have a limited size in the z -direction.

2.2 MHD equations

We perform 2.5-dimensional ($\partial/\partial z = 0$) numerical simulations in the Cartesian coordinates as described above. The MHD equations are slightly modified from Chen et al. (1999a,b) in order to include the gravity from both stars and the centrifugal force in the co-rotating system. For simplicity, heat conduction is not included. The resulting dimensionless MHD equations, which are shown below, are numerically solved by a multistep implicit scheme (Hu 1989; Chen, Fang & Hu 2000).

$$\frac{\partial \rho}{\partial t} + v_x \frac{\partial \rho}{\partial x} + v_y \frac{\partial \rho}{\partial y} + \rho \frac{\partial v_x}{\partial x} + \rho \frac{\partial v_y}{\partial y} = 0, \quad (1)$$

$$\frac{\partial v_x}{\partial t} + v_x \frac{\partial v_x}{\partial x} + v_y \frac{\partial v_x}{\partial y} + \frac{T}{\rho} \frac{\partial \rho}{\partial x} + \frac{\partial T}{\partial x} + \frac{2B_z}{\rho\beta_0} \frac{\partial B_z}{\partial x} + \frac{2}{\rho\beta_0} \frac{\partial \psi}{\partial x} \Delta\psi - g - F_c = 0, \quad (2)$$

$$\frac{\partial v_y}{\partial t} + v_x \frac{\partial v_y}{\partial x} + v_y \frac{\partial v_y}{\partial y} + \frac{\partial T}{\partial y} + \frac{T}{\rho} \frac{\partial \rho}{\partial y} + \frac{2}{\rho\beta_0} \frac{\partial \psi}{\partial y} \Delta\psi + \frac{2B_z}{\rho\beta_0} \frac{\partial B_z}{\partial y} = 0, \quad (3)$$

$$\frac{\partial v_z}{\partial t} + v_x \frac{\partial v_z}{\partial x} + v_y \frac{\partial v_z}{\partial y} + \frac{2}{\rho\beta_0} \frac{\partial \psi}{\partial x} \frac{\partial B_z}{\partial y} - \frac{2}{\rho\beta_0} \frac{\partial \psi}{\partial y} \frac{\partial B_z}{\partial x} = 0, \quad (4)$$

$$\frac{\partial \psi}{\partial t} + v_x \frac{\partial \psi}{\partial x} + v_y \frac{\partial \psi}{\partial y} - \frac{1}{R_m} \Delta\psi = 0, \quad (5)$$

$$\frac{\partial B_z}{\partial t} - \frac{\partial v_z}{\partial x} \frac{\partial \psi}{\partial y} + \frac{\partial v_z}{\partial y} \frac{\partial \psi}{\partial x} + B_z \frac{\partial v_x}{\partial x} + B_z \frac{\partial v_y}{\partial y} + v_x \frac{\partial B_z}{\partial x} + v_y \frac{\partial B_z}{\partial y} - \frac{\partial}{\partial x} \left(\frac{1}{R_m} \frac{\partial B_z}{\partial x} \right)$$

$$\frac{\partial T}{\partial t} + v_x \frac{\partial T}{\partial x} + v_y \frac{\partial T}{\partial y} + (\gamma - 1)T \frac{\partial v_x}{\partial x} + (\gamma - 1)T \frac{\partial v_y}{\partial y} - \frac{2(\gamma - 1)}{\rho\beta_0 R_m} \left[\left(\frac{\partial B_z}{\partial x} \right)^2 + \left(\frac{\partial B_z}{\partial y} \right)^2 \right]$$

where ρ , v_x , v_y , v_z , ψ , B_z and T correspond to the dimensionless density, three components of velocity, magnetic flux function, z -component of the magnetic strength, and temperature, respectively, and ρ_0 , v_0 , ψ_0 , B_0 and T_0 are the characteristic values of the corresponding parameters, which are used to nondimensionalize the equations. The characteristic velocity v_0 is defined as the isothermal sound speed $v_0 = \sqrt{RT_0}$, where R is the gas constant for the fully ionised hydrogen and the length scale L_0 is set to be $0.5 R_\odot$. The dimensionless size of the simulation box is then $0 \leq |y| \leq 5$ and $0 \leq x \leq 5.26$. Since the flux function and the magnetic field are related by

$$\mathbf{B} = \nabla \times (\psi \mathbf{e}_z) + B_z \mathbf{e}_z, \quad (8)$$

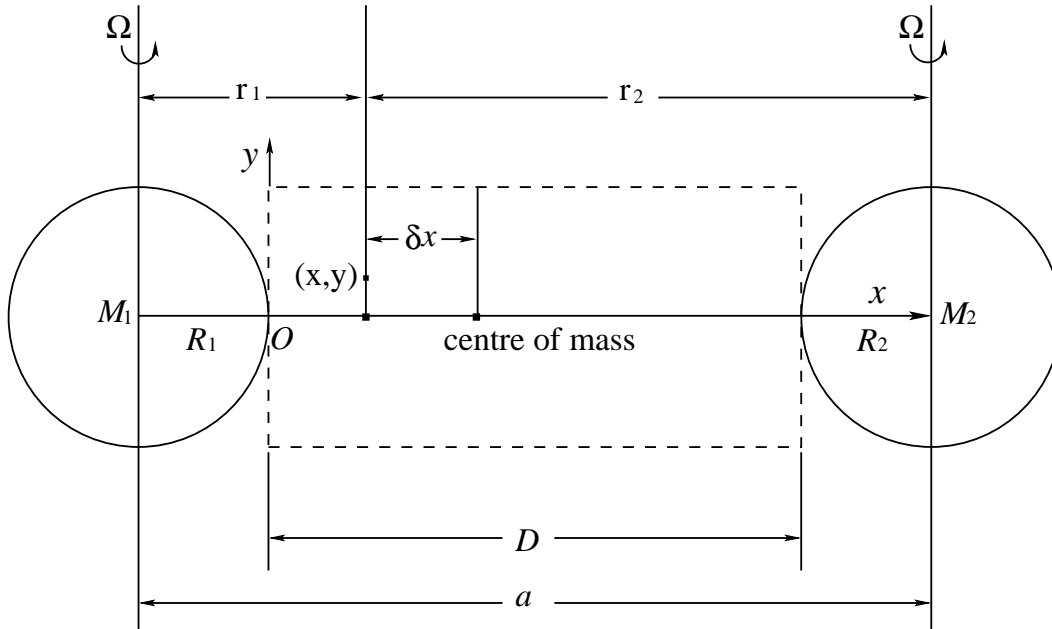


Figure 1. Sketch of the binary system. For the case of YY Gem, the two stars are identical. Here, δx is the deviation of the x -coordinate from the centre of mass, r_1 is the distance to the centre of M_1 , and r_2 is the distance to the centre of M_2 . The simulation box is indicated by the dashed box.

where e_z is the unit vector in the z -axis, we have $\psi_0 = B_0 L_0$.

In equation (2), g is the total acceleration of gravity contributed by both stars,

$$g = \frac{G}{v_0^2 L_0} \left(\frac{M_2}{r_2^2} - \frac{M_1}{r_1^2} \right), \quad (9)$$

where M_1 and M_2 are the masses of the two stars, r_1 and r_2 are indicated in Fig. 1 (note that such an expression is an extension of the gravity along the x -axis, which is valid since we are interested in the processes near the x -axis). In the same equation, F_c represents the centrifugal force,

$$F_c = \frac{G(M_1 + M_2)L_0^2}{v_0^2 a^3} \delta x, \quad (10)$$

where a is the distance between the two stars, δx is the deviation of the x -coordinate from the centre of mass. The plasma beta, β_0 , and the magnetic Reynolds number, R_m , are expressed as

$$\beta_0 = \frac{2\mu_0 \rho_0 v_0^2}{B_0^2}, \quad (11)$$

$$R_m = \frac{\mu_0 v_0 L_0}{\eta}, \quad (12)$$

where μ_0 is the magnetic permeability and η is the anomalous resistivity. Similarly to Chen & Priest (2006), η is chosen to be a function of the current density, j ,

$$\eta = \begin{cases} \eta_0 \min(1, j/j_c - 1), & j \geq j_c, \\ 0, & j < j_c, \end{cases} \quad (13)$$

where j_c is the critical current density.

The time unit used in the description of the numerical results is the Alfvén time-scale, $\tau_A = L_0/v_A$, where v_A is Alfvén speed, i.e.,

$$v_A = \frac{\psi_0}{L_0 \sqrt{\mu_0 \rho_0}}. \quad (14)$$

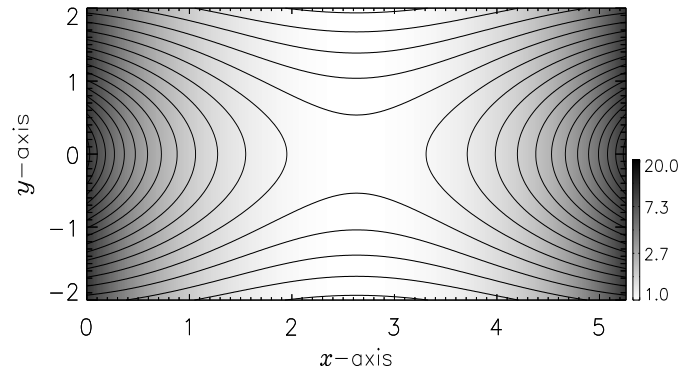


Figure 2. Initial configuration of the magnetic field (solid lines) and the distribution of the dimensionless density (gray scale).

As Tsikoudi & Kellett (2000) pointed out, the corona of YY Gem is very hot, T_0 can be taken to be several million kelvin. The number density ($n = \rho/m_p$) of the stellar corona is in the range of $10^{14} - 10^{18} \text{ m}^{-3}$ (Monsignor-Fossi & Landini 1994; Mewe et al. 1995; Schmitt et al. 1996; Schrijver & Zwaan 2000; Ness et al. 2002). The typical strength of the general magnetic field near the stellar surface is tens of Gauss. Therefore, in our standard case, which is called case A2 later, the following characteristic values are adopted: $n_0 = 10^{15} \text{ m}^{-3}$, $T_0 = 1.9 \times 10^6 \text{ K}$, $\beta_0 = 0.01$ (hence $B_0 = 36 \text{ G}$), and $j_c = 10$. The corresponding time-scale is $\tau_A = 139 \text{ s}$.

2.3 Initial and boundary conditions

Initially, the isothermal plasma is at rest, i.e., $v_x = v_y = v_z = 0$, and $T = 1$. The density distribution is obtained by numerically calculating the hydrostatic equation

$$\frac{1}{\rho} \frac{d\rho}{dx} = g(x) + F_c(x). \quad (15)$$

The initial magnetic field in this work is assumed to be potential, which is produced by two parallel line currents lying below the two surfaces, i.e.,

$$\psi = -\ln(\sqrt{(x-x_1)^2+y^2}) - \ln(\sqrt{(x-x_2)^2+y^2}), \quad (16)$$

where x_1 and x_2 are the x -coordinates of these two currents. We take $x_1 = -1$ and $x_2 = D/L_0 + 1$ in our work. The resulting density distribution and the magnetic configuration are plotted in Fig. 2, where the magnetic field is similar to the configuration adopted in Ferreira (1998). The magnetic configuration is taken in such a way that a magnetic null point exists between the antiparallel magnetic loops. So, whenever the closed loops bulge, a current sheet forms naturally, and magnetic reconnection is ready to commence (if the polarity of one magnetic system expressed in equation (16) is flipped, the two loop systems become to repel each other, and no reconnection can happen). Similar magnetic connectivity with a null point was also computed for the active RS CVn system (Uchida & Sakurai 1983; Uchida & Sakurai 1985; Beasley & Güdel 2000).

Owing to the symmetry, calculations are done only in the upper half of the simulation area, i.e., $0 \leq x \leq D$ and $0 \leq y \leq 2.5 R_\odot$. The calculation domain is discretised into 501 uniform grid points along the x -axis and 141 nonuniform grid points along the y -axis, with more grid points concentrated near the x -axis. The top side of the simulation box ($y = 5$) is treated as an open boundary, and the bottom one ($y = 0$) is a symmetry boundary. The right and left, which correspond to the surface of the binary stars, are line-tied boundaries, where all quantities are fixed except that a typical differential rotation is imposed at each surface in the following form:

$$v_z|_{\text{left}} = \begin{cases} -\Omega R(1 - \alpha \sin^2 i) \sqrt{1 - \sin^2 i} + \Omega R, & i \leq \pi/2, \\ \Omega R, & i > \pi/2, \end{cases} \quad (17)$$

$$v_z|_{\text{right}} = \begin{cases} \Omega R(1 - \alpha \sin^2 i) \sqrt{1 - \sin^2 i} - \Omega R, & i \leq \pi/2, \\ -\Omega R, & i > \pi/2, \end{cases} \quad (18)$$

where Ω is the angular velocity of the binary, α is the differential rotation rate, and i , the latitude, is related to the coordinate y by $y = R \sin i$. Beyond $y = R$, v_z is set to be the value at $y = R$. In this paper, α is set to be 0.5. As we will discuss later, the value of α does not affect the main results in our numerical simulations.

3 NUMERICAL RESULTS

3.1 General evolution

The distributions of the magnetic field, the temperature, and the velocity field at several selected times in case A2 are shown in Fig. 3. As the shear motion is imposed at the left and right boundaries, footpoints of the coronal loops are dragged to move in the z -direction, which increases the local magnetic pressure. As a result, both the left and the right magnetic loop systems begin to inflate and approach each other due to the increasing pressures near the roots of the loop systems (see the snapshot at $t = 83 \tau_A$). Such an

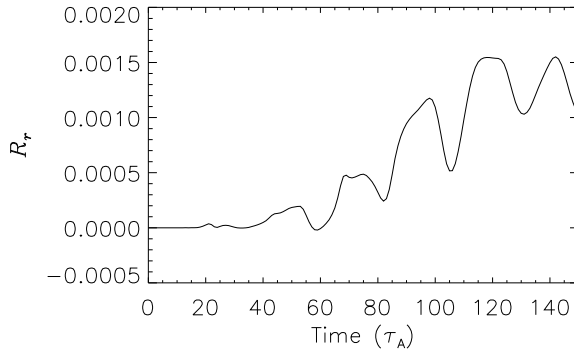


Figure 4. Temporal evolution of the reconnection rate in case A2, where R_r is the reconnection rate, and $\tau_A = 139$ s.

inflation of magnetic loops due to shear motions was demonstrated on the Sun (Barnes & Sturrock 1972). The two loop systems collide near the magnetic null point, by which a current sheet forms. When the increasing current density exceeds the prescribed threshold (j_c), anomalous resistivity is excited, which triggers the occurrence of magnetic reconnection between the two loop systems (see the snapshot at $t = 109 \tau_A$). The temporal evolution of the reconnection rate, R_r , which is defined as $d\psi/dt$ at the magnetic null point, is shown in Fig. 4. It is seen that the reconnection rate presents a periodic behaviour. With the wavelet analysis, the period is found to be 54 ± 6 min. Note that, with the 2.5D approximation in our model, the reconnection between the two closed magnetic systems, which are rooted on the surfaces of the binary stars, will go on as long as the differential rotation continues. In reality, the differential rotation of the two spherical stellar surfaces would take the two closed magnetic systems apart, which would cease the reconnection after a certain time. The 2.5D model is valid here since we are interested in the magnetic reconnection only during first several periods.

In order to compare the numerical result with the U -band observations made by Doyle et al. (1990), we synthesised the UV emission in the wave-band of $3650 \pm 10 \text{ \AA}$ from our numerical results with the help of the CHIANTI database (Dere et al. 1997; Landi et al. 2006; see Chen & Priest 2006 for details). The calculated UV light-curve of the whole simulation area is plotted in the left panel of Fig. 5, and its wavelet spectrum is presented in the right panel. Note that since the reconnection rate and the UV emission both are small in the first $60 \tau_A$, we displayed the result after $t = 60 \tau_A$. It is seen that the UV flux does show a periodicity, and the period is centred at 52 min, very close to that of the reconnection rate, i.e., 54 min.

3.2 Parameter survey

In order to investigate how the choice of the characteristic values of various parameters may affect the results, we have made numerical simulations with different characteristic values, which are listed in Table 1. In cases A1–A5, only T_0 is changed. Similarly, cases B1–B5 are for β_0 dependence, cases C1–C3 for ρ_0 , and cases D1–D3 for j_c , respectively. In all cases, L_0 is fixed to be $0.5 R_\odot$. Numerical simulations

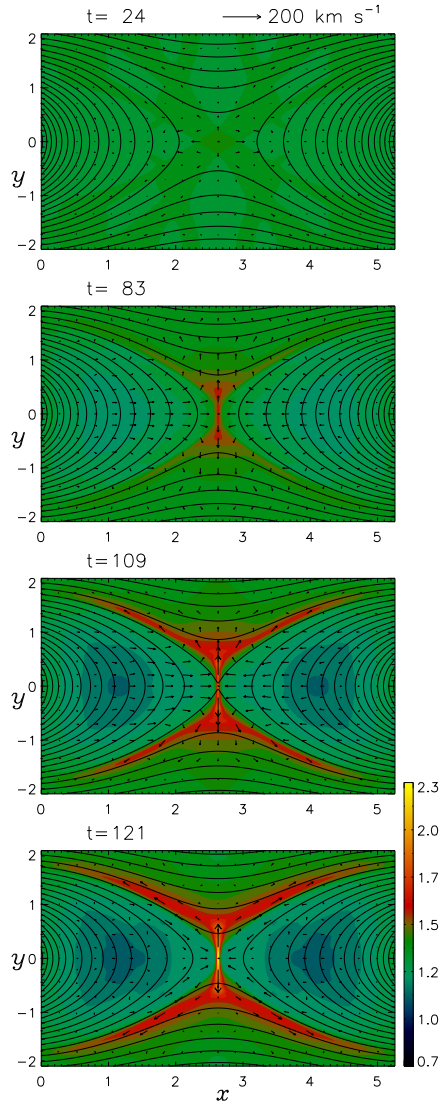


Figure 3. Magnetic field lines (solid lines), velocities (arrows), and temperatures (colour) at five selected times in case A2.

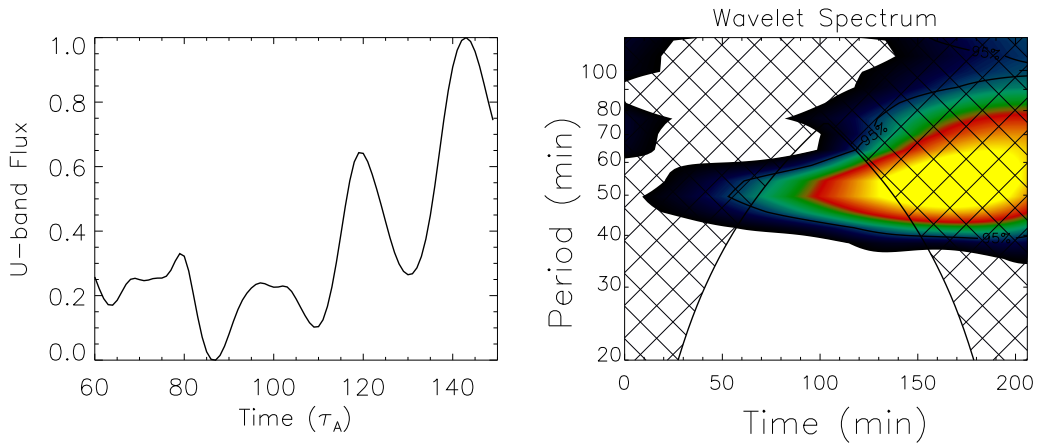


Figure 5. Left panel: Temporal evolution of the flux in the U -band, which is derived by using the CHIANTI database. Right panel: The wavelet spectrum corresponding to the U -band flux, which has a period centred around about 52 min.

Table 1. Parameters used in different simulation cases.

| Models | T_0 ($\times 10^6$ K) | β_0 | $\lg n_0/\text{m}^{-3}$ | j_c | P (min) |
|--------|--------------------------|-----------|-------------------------|-------|-------------|
| A1 | 1.5 | 0.01 | 15 | 10.0 | 70 ± 9 |
| A2 | 1.9 | 0.01 | 15 | 10.0 | 54 ± 6 |
| A3 | 2.5 | 0.01 | 15 | 10.0 | 41 ± 4 |
| A4 | 3.0 | 0.01 | 15 | 10.0 | 35 ± 3 |
| A5 | 4.0 | 0.01 | 15 | 10.0 | 31 ± 3 |
| <hr/> | | | | | |
| B1 | 2.0 | 0.05 | 15 | 10.0 | 96 ± 15 |
| B2 | 2.0 | 0.025 | 15 | 10.0 | 78 ± 10 |
| B3 | 2.0 | 0.01 | 15 | 10.0 | 52 ± 6 |
| B4 | 2.0 | 0.0075 | 15 | 10.0 | 47 ± 4 |
| B5 | 2.0 | 0.005 | 15 | 10.0 | 38 ± 4 |
| <hr/> | | | | | |
| C1 | 2.0 | 0.01 | 14 | 10.0 | 52 ± 6 |
| C2 | 2.0 | 0.01 | 15 | 10.0 | 52 ± 6 |
| C3 | 2.0 | 0.01 | 16 | 10.0 | 52 ± 6 |
| <hr/> | | | | | |
| D1 | 2.0 | 0.01 | 15 | 1.0 | 52 ± 6 |
| D2 | 2.0 | 0.01 | 15 | 5.0 | 52 ± 6 |
| D3 | 2.0 | 0.01 | 15 | 10.0 | 52 ± 6 |

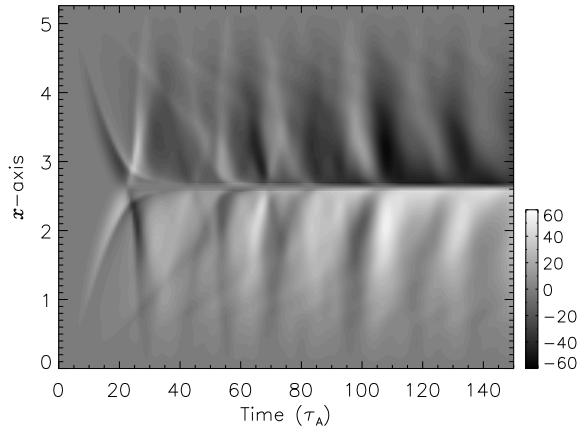
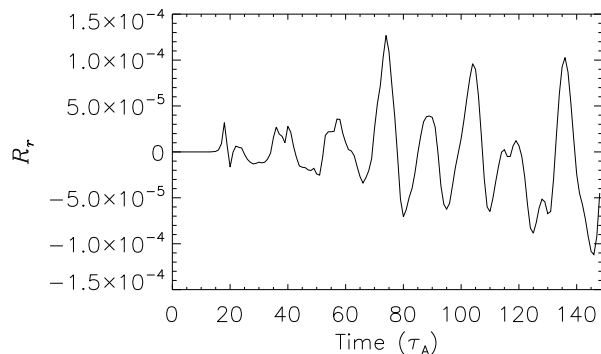
indicate that, similar to case A2 as described in the previous subsection, all other cases present periodic behaviours. The corresponding period of each case is displayed in the last column of Table 1. It is found that, with T_0 , β_0 , ρ_0 , and j_c as independent parameters, the period of the flaring is strongly dependent on T_0 and β_0 , and an increasing T_0 or decreasing β_0 results in a decreasing period. When ρ_0 increases, the magnetic field B_0 increases as well in order to keep β_0 constant (correspondingly, the Alfvén speed is constant). As a result, the period of the reconnection rate does not change. It is also seen from Table 1 that j_c has little effect on the period, which implies that the magnetic reconnection is modulated by some external process.

Besides the four parameters mentioned above, we also examine other parameters related to the binary itself. In case A2, by changing the values of α ($\alpha = 0.2, 0.3, 0.4, 0.5, 0.6, 0.7, 0.8$), we find that the results keep invariant, i.e., $P = 54 \pm 6$ min. In other words, the flaring period has nothing to do with the speed of the differential rotation. As mentioned above, the mass and the size of YY Gem are taken from Brancewicz & Dworak (1980). However, other authors derived slightly different values (Leung & Schneider 1978; Chabrier & Baraffe 1995; Torres & Ribas 2002), e.g., in Leung & Schneider (1978), $M_1 = 0.62 M_\odot$, $M_2 = 0.57 M_\odot$, $R_1 = 0.66 R_\odot$, $R_2 = 0.58 R_\odot$, the separation of two components $a = 3.9 R_\odot$, and the orbital period $P = 0.82$ d. Through test calculations, we find little change in the results.

4 DISCUSSIONS

4.1 What modulates the magnetic reconnection?

In order to understand how the magnetic reconnection is modulated, the temporal evolution of v_x along the x -axis is shown in Fig. 6, where the value of v_x is indicated by the grey scales. As the reconnection rate R_r is equivalent to $v_x B_y$ along the x -axis, it is expected to see that v_x at a given point also shows an oscillatory evolution, with the same period as R_r , i.e., 54 min. Furthermore, a wave pattern

**Figure 6.** Temporal evolution of v_x along the x -axis.**Figure 7.** Temporal evolution of reconnection rate in the case that the horizontal size of the simulation box is cut down.

is discerned in Fig. 6, where the waves are seen to travel back and forth in the x -direction, bounded by the surfaces of the two stars. Since the waves propagate perpendicular to the magnetic field lines, we postulate that they are fast-mode magnetoacoustic waves, and that the periodic magnetic reconnection in the numerical results is modulated by such waves.

To verify that the magnetic reconnection is modulated by magnetoacoustic waves bouncing back and forth between the two stellar surfaces, we shift the right boundary of case A2 leftward and the left boundary rightward by 0.8 simultaneously, by which the separation between the two stellar surfaces is cut down from 5.26 to 3.66, i.e., a decrease with a ratio of 30 per cent. The corresponding evolution of the reconnection rate is plotted in Fig. 7. Note that the positive R_r means that the field lines in the two loop systems are reconnecting, whereas the negative R_r means that the transverse field lines are reconnecting.

It is found that the resulting period of magnetic reconnection becomes 34 ± 6 min. This means that the period decreases by 37 per cent, a ratio close to that of the decrease of the separation between the two stellar surfaces. This implies that the magnetic reconnection is modulated by waves trapped between the two stellar surfaces.

To verify that the travelling waves are fast-mode waves,

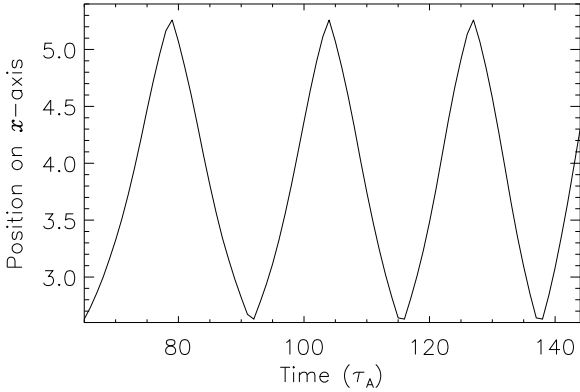


Figure 8. Temporal evolution of the wave front. Only the right half is plotted owing to the symmetry of the YY Gem system.

here we calculate the trajectory of fast-mode waves propagating from the reconnection point ($x = 2.63$), through the right boundary ($x = 5.26$) and then back to the reconnection point along the x -axis. For a given number n , the travelling time (T) and the position of the wave front (x) are determined by the following equations

$$T = \sum_{i \geq 1}^n \Delta x / v_f, \quad x - 2.63 = \sum_{i \geq 1}^n \Delta x, \quad (19)$$

where Δx is the uniform grid spacing in the x -direction, and v_f is the fast-mode wave velocity. The procedure is described as follows: Starting from the reconnection point ($x=2.63$), the wave front propagates rightward by Δx each step, the time interval Δt is equal to Δx divided by v_f , so the total travelling time is the sum of Δt , while the position is the sum of Δx . Note that since both the magnetic field and the plasma temperature are changing with time, we update the magnetic and thermal parameters every $1 \tau_A$ when calculating v_f . Besides, when the wave reaches the right boundary and then bounces back, Δx takes a negative value. After the wave front returns to the reconnection point, the wave should propagate to the left half area of the simulation box. Considering the symmetry of the problem, i.e., there is a symmetric wave propagating rightward from the left half area, we repeat the above calculation in the right half region.

Figure. 8 shows the temporal evolution of the position of the wave front in the right half region only. It is found that the trajectory of the fast-mode wave, from the reconnection point to the right (or left) boundary and then back to the reconnection point, is quasi-periodic, with a period of $\sim 23 \pm 2 \tau_A$, i.e., $\sim 53 \pm 5$ min, very close to the period of the magnetic reconnection rate presented in Section 3. Therefore, we are convinced that the magnetic reconnection is modulated by fast-mode waves. The underlying process can be understood as follows: When symmetric waves, introduced either by the shear motions of the stellar surfaces or by the magnetic reconnection, collide near the reconnection point, the reconnection rate is enhanced to form a peak. After the collision, the two waves propagate to the right and left boundaries and are bounced back, respectively. When they collide again near the reconnection point, the reconnection rate is enhanced again. Therefore, the period of the

magnetic reconnection is determined by the travelling time of fast-mode waves from the reconnection point to the right (or left) boundary and then back to the reconnection point.

4.2 Empirical formula for the period

As shown in Section 3, among the selected four parameters, the period of the reconnection rate (P) is explicitly dependent on T_0 and β_0 . The underlying process can be understood as follows: When T_0 increases while keeping β_0 and ρ_0 constant, both the sound speed and the Alfvén speed increase, which leads to a larger fast-mode wave speed. As a result, the period of the reconnection rate decreases; When β_0 decreases while keeping T_0 and ρ_0 constant, the sound speed does not change, while the Alfvén speed increases, which also leads to a larger fast-mode wave speed and a shorter period; When ρ_0 increases while keeping β_0 and T_0 constant, both the sound and the Alfvén speed do not change (the Alfvén speed does not change since the magnetic field B_0 increases). As a result, the period keeps constant.

In order to derive an empirical formula to relate P to T_0 and β_0 , we simulate a series of cases with different T_0 and β_0 . The corresponding variations of P with T_0 and β_0 are displayed by the squares in Fig. 9. It is seen that $\lg P$ is almost a linear function of $\lg T_0$ and $\lg \beta_0$, which means that P scales with T_0 and β_0 as $P \propto T_0^{\gamma_1} \beta_0^{\gamma_2}$. By fitting the data points with the solid lines in Fig. 9, we obtain $\gamma_1 = -0.91$ and $\gamma_2 = 0.42$. Therefore, we have $P \propto T_0^{-0.91} \beta_0^{0.42}$, i.e.,

$$P \sim \rho_0^{0.42} T_0^{-0.49} B_0^{-0.84}. \quad (20)$$

According to our postulation that the magnetic reconnection is modulated by fast-mode waves, the period P should be proportional to $1/v_f$, where $v_f^2 = c_s^2 + v_A^2$, $c_s^2 = \gamma R T_0$, and $v_A^2 = B_0^2 / (\mu_0 \rho_0)$. In the extreme case of zero magnetic field, we have $P \propto T_0^{-0.5}$; In the case of extremely strong magnetic field, we have $P \propto \rho_0^{0.5} B_0^{-1}$. The slight deviation of the power indices in our numerical results from those in the two extreme cases further implies that it is the fast-mode waves that modulate the magnetic reconnection. Based on this scaling law, the observed period of the flaring rate in YY Gem, i.e., 48 min, corresponds to a characteristic magnetic field of 41 G, which is the value of the magnetic field in low corona, providing the number density of the plasma in the inter-binary space is about $n_0 \sim 10^{15} \text{ m}^{-3}$.

4.3 Other points

The periodic flaring of YY Gem, which was found by Doyle et al. (1990), was not confirmed in Stelzer et al. (2002). The discrepancy might be attributed to two factors: (1) Probably the two observations were made at different phases of the stellar magnetic cycle. In order to have the large-scale magnetic reconnection in the inter-binary space, the magnetic configuration of each star should be close to the bipolar type, with interconnecting magnetic field lines linking the polar regions of the binary stars, as shown by Fig. 2. Such a magnetic configuration often appears near activity minimum; (2) The periodic flares observed by Doyle et al. (1990) and confirmed by our numerical simulations, are produced in the inter-binary space, therefore, are large-scale in

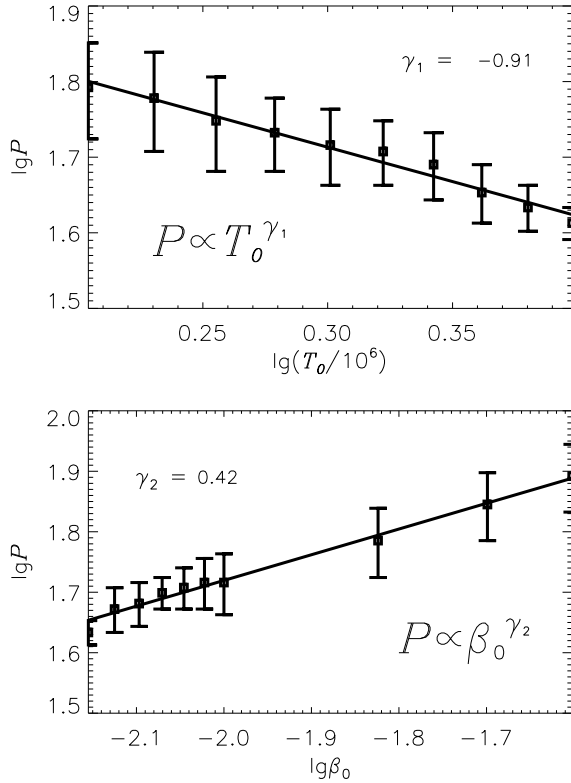


Figure 9. Upper panel: Relation between the period (P) and the temperature (T); Lower panel: Relation between the period (P) and β_0 . The solid lines are the corresponding linear fitting of the data points.

nature. Without doubt, there should be small-scale flares that occur near the stellar surface and are due to the reconnection of the magnetic fields of an individual star. The flares observed by Stelzer et al. (2002) probably correspond to these small-scale flares.

5 CONCLUSIONS

Observations indicated that there may exist periodicity in the occurrence of strong flares from YY Gem. Using 2.5-dimensional MHD numerical simulations, we confirmed the periodicity of the flaring in the inter-binary space of YY Gem. On the basis of the analysis of the simulation results, the following conclusions can be drawn:

1. Owing to the differential rotation of the stellar surface, coronal loops in each star inflate and approach each other. The resulting magnetic reconnection generates the inter-binary flares, which are large-scale in nature. Fast magnetoacoustic waves, which are trapped in the inter-binary space between the surfaces of the two binary components, modulate the magnetic reconnection, producing the periodic behaviour of the flaring rate.

2. The period scales with the typical coronal density (ρ_0), temperature (T_0), and the coronal magnetic field (B_0) as $P \sim \rho_0^{0.42} T_0^{-0.49} B_0^{-0.84}$.

ACKNOWLEDGMENTS

We thank the referee for constructive comments that led to an improvement of the paper. We are also grateful to C. Fang, X. Y. Xu, M. Jin, and Q. M. Zhang for their helpful suggestions. This work was supported by the Chinese foundations NCET-04-0445, FANEDD (200226), NSFC under grants 10025315, 10221001, 10333040, 10403003, and 10673004, and by NKBRF under grant 2006CB806302.

REFERENCES

- Adams W. S., Joy A. H., 1920, *PASP.*, 32, 158
 Barnes C. W., Sturrock P. A., 1972, *ApJ*, 174, 659
 Beasley A. J., Güdel M., 2000, *ApJ*, 529, 961
 Brancewicz H. K., Dworak T. Z., 1980, *Acta Astronomica*, 30, 501
 Butler C. J., Doyle J. G., Budding E., 1996, in Pallavicini R., Dupree A. K., eds, *Cool Stars, Stellar Systems, and the Sun* Vol. 109 of *Astronomical Society of the Pacific Conference Series*, Surface inhomogeneities on YY Geminorum. p 589
 Chabrier G., Baraffe I., 1995, *ApJ*, 451, L29
 Chen P. F., Fang C., Ding M. D., Tang Y. H., 1999a, *ApJ*, 520, 853
 Chen, P. F., Fang, C., Hu, Y. Q., 2000, *Chin. Sci. Bull.*, 45, 798
 Chen P. F., Fang C., Tang Y. H., Ding M. D., 1999b, *ApJ*, 513, 516
 Chen P. F., Priest E. R., 2006, *Sol. Phys.*, 238, 313
 Cheng C.-C., Pallavicini R., 1991, *ApJ*, 381, 234
 Culhane J. L., White N. E., Parmar A. N., Shafer R. A., 1990, *MNRAS*, 243, 424
 Dere, K. P., Landi, E., Mason, H.E. et al., 1997, *Astron. Astrophys. Suppl.*, 125, 149
 Doyle J. G., Butler C. J., 1985, *Nat*, 313, 378
 Doyle J. G., Butler C. J., van den Oord G. H. J., Kiang T., 1990, *A&A*, 232, 83
 Doyle J. G., Mathioudakis M., 1990, *A&A*, 227, 130
 Dworak T. Z., 1975, *Acta Astronomica*, 25, 383
 Ferreira J. M., 1998, *A&A*, 335, 248
 Haisch B. M., Schmitt J. H. M. M., Rodono M., Gibson D. M., 1990, *A&A*, 230, 419
 Hu Y. Q., 1989, *J. Comput. Phys.*, 84, 441
 Jackson P. D., Kundu M. R., White S. M., 1989, *A&A*, 210, 284
 Joy A. H., Sanford R. F., 1926, *ApJ*, 64, 250
 Kron G. E., 1952, *ApJ*, 115, 301
 Landi E., Del Zanna, G., Young, P.R. et al., 2006, *ApJS*, 162, 261
 Leung K.-C., Schneider D. P., 1978, *AJ*, 83, 618
 Mewe R., Kaastra J. S., Schrijver C. J., van den Oord G. H. J., Alkemade F. J. M., 1995, *A&A*, 296, 477
 Moffett T. J., 1974, *ApJS*, 29, 1
 Moffett T. J., Bopp B. W., 1971, *ApJ*, 168, L117
 Monsignor-Fossi B. C., Landini M., 1994, *A&A*, 284, 900
 Nakariakov V. M., Foullon C., Verwichte E., Young N. P., 2006, *A&A*, 452, 343
 Ness J.-U., Schmitt J. H. M. M., Burwitz V., Mewe R., Raassen A. J. J., van der Meer R. L. J., Predehl P., Brinkman A. C., 2002, *A&A*, 394, 911

- Pres P., Siarkowski M., Sylwester J., 1995, MNRAS, 275, 43
- Qian S. B., Liu D. L., Tan W. L., Soonthornthum B., 2002, AJ, 124, 1060
- Saar S. H., Bookbinder J. A., 2003, in Brown A., Harper G. M., Ayres T. R., eds, *The Future of Cool-Star Astrophysics: 12th Cambridge Workshop on Cool Stars, Stellar Systems, and the Sun* (University of Colorado), Vol. 12, STIS Far UV Studies of Spatial and Temporal Activity Variations in YY Gem. pp 1020–1023
- Schmitt J. H. M. M., Drake J. J., Haisch B. M., Stern R. A., 1996, ApJ, 467, 841
- Schrijver C. J., Zwaan C., 2000, *Solar and Stellar Magnetic Activity*. Cambridge Univ. Press, United Kingdom, p. 263
- Siarkowski M., 1992, MNRAS, 259, 453
- Siarkowski M., Pres P., Drake S. A., White N. E., Singh K. P., 1996, ApJ, 473, 470
- Stelzer B., Burwitz V., Audard M., Güdel M., Ness J.-U., Grosso N., Neuhäuser R., Schmitt J. H. M. M., Predehl P., Aschenbach B., 2002, A&A, 392, 585
- Struve O., Zebergs V., 1959, ApJ, 130, 783
- Torres Guillermo, Ribas Ignasi, 2002, ApJ, 567, 1140
- Tsikoudi V., Kellett B. J., 2000, MNRAS, 319, 1147
- Uchida Y., Sakurai T., 1983, in Byrne P. B., Rodono M., eds, *IAU Colloq. 71: Activity in Red-Dwarf Stars Vol. 102 of Astrophysics and Space Science Library, Interacting magnetospheres in RS CVn binaries - Coronal heating and flares*. pp 629–632
- Uchida Y., Sakurai T., 1985, in Kundu M. R., Holman G. D., eds, *Unstable Current Systems and Plasma Instabilities in Astrophysics Vol. 107 of IAU Symposium, Magnetodynamical processes in interacting magnetospheres of RS CVn binaries*. pp 281–285
- van Gent H., 1931, BAN., 6, 99

This paper has been typeset from a $\text{T}_{\text{E}}\text{X}/\text{L}^{\text{A}}\text{T}_{\text{E}}\text{X}$ file prepared by the author.